*Manuscript in PDF

Available online at www.sciencedirect.com

ScienceDirect

Procedia CIRP 00 (2018) 000–000

www.elsevier.com/locate/procedia

51st CIRP Conference on Manufacturing Systems

On motion planning for narrow-clearance assemblies using virtual manikins

Yi Li[a,*], Niclas Delfs[a], Peter Mårdberg[a], Robert Bohlin[a], Johan S. Carlson[a]

[a] *Fraunhofer-Chalmers Research Centre for Industrial Mathematics, Gothenburg 41288, Sweden*

[*] Corresponding author. Tel.: +46-31-7724244; fax: +46-31-7724260. *E-mail address:* yi.li@fcc.chalmers.se

Abstract

Digital Human Modeling (DHM) is an important tool to improve assembly ergonomics and thereby also productivity and product quality. State-of-art DHM tools can simulate challenging assembly operations by solving inverse kinematic problems so that the positions/orientations of the hands/feet of a manikin match some manually-specified targets. However, it is still difficult and time-consuming for a simulation engineer to perform an assembly with narrow insertion clearances by manually setting hand targets. We present a novel and highly automated approach that explores the 4D space (position of a fingertip plus pronation/supination of the arm) around an initial path for a sphere.
© 2018 The Authors. Published by Elsevier B.V.
Peer-review under responsibility of the scientific committee of the 51st CIRP Conference on Manufacturing Systems.

Keywords: Advanced Biomechanical Models; Assembly Simulation; Digital Human Models; Ergonomics; Optimization; Visualization

1. Introduction

Today, manual assembly still remains a large part of the final assembly process in manufacturing industries. Consequently, it is important to use Digital Human Modeling (DHM) tools to analyze human postures and motions in order to evaluate both human-product interactions and human-production system interactions and then predict ergonomics issues before the product and workplace exist physically. Whenever poor assembly ergonomics concepts and poor system solutions are identified from the study, they should be redesigned to keep the ergonomics-related cost down [1].

With the addition of a user-friendly and non-expert DHM tool called IMMA (Intelligently Moving Manikins) [2], it is now possible to synthesize collision-free and ergonomic motions for a system consisting of a manikin and the part being assembled (e.g., a task sequence to assemble a door panel in a truck) using the manikin motion generator inside IMMA.

During assembly process, a worker may have to thrust his/her hand into a narrow gap between two parts in an assembly (e.g., to fasten a screw connection). Therefore, before the product design is finalized, it is important to use a DHM tool to verify that the gap between the parts is accessible to a human hand (or at least fingers). In effect, we want to synthesize a goal configuration with the manikin's hand inside the narrow gap and then generate a sequence of collision-free motions that takes the manikin from its initial configuration to the goal configuration, where the *configuration* of a manikin is a complete specification of the position of every point of that manikin [3]. In this paper, we make the assumption that the worker's hand does not hold a tool.

This paper is organized as follows. After discussing the related work in Section 2, the IMMA manikin model is briefly presented in Section 3. In Section 4, we present our approach to synthesize not only a goal configuration with the manikin's hand inside the narrow gap, but also a sequence of collision-free manikin motions between the initial and goal configurations. Moreover, our successful experimental results are shown in Section 5. Finally, some discussions, conclusions, and directions for future research are provided in Sections 6 and 7.

2. Related Work

The problem of generating collision-free motions for digital humans has been extensively studied by researchers in different fields such as robotics and computer graphics. For example, the goal of motion planning in the field of robotics is to find collision-free and continuous motions between the initial and goal configurations.

Actual human motions can be captured using motion capture (MoCap) technology. However, marker-based MoCap systems are very expensive and difficult to set up, whereas marker-free systems are not very accurate and expensive too [4]. Furthermore, even though captured motions can be combined to generate new ones for a given virtual environment [5,6], it is difficult to achieve precision motions required for constrained environments such as vehicle assembly lines. When applying manual dexterity to tasks such as grasping [7,8] and manipulating objects, hand-tracking devices can be employed. Hand motion measurement systems come in two forms: wearable glove-type

2212-8271 © 2018 The Authors. Published by Elsevier B.V.
Peer-review under responsibility of the scientific committee of the 51st CIRP Conference on Manufacturing Systems.

and nonglove-type [9]. Nevertheless, neither of these two types of systems is able to accurately measure the fingers' joint angles.

Instead, IMMA defines the motions using mathematics and optimization techniques similar to automatic path planning algorithms developed in the field of robotics and it is able to take into account kinematic constraints, balance, contact forces, and comfort when synthesizing assembly motions for manikins. Assuming that the manikin starts in a collision-free configuration, IMMA is able to prevent the manikin to come too close to the obstacles using an obstacle repulsive potential field [10]. The field is not able to free the manikin from collision though.

Most existing DHM tools require theirs users to manipulate the manikin joint by joint [2], although this manual adjustment process not only is time-consuming but also leads to inconsistent posture and motion results both within and between tool users. Instead of manipulate the joints manually, an IMMA user only needs to specify a sequence of target frames for e.g., a hand. However, due to the obstacle repulsive potential field from the parts, it may be very difficult for the IMMA user to specify the exact target frames required for bringing in the hand into a narrow gap. The much more likely outcome is that the hand is pushed aside by the repulsive potential field when it is getting close to the narrow gap. Furthermore, when target frames are selected manually, it is difficult to guarantee reproducibility.

In the field of robotics, sampling-based approaches such as the Probabilistic Roadmap (PRM) [11] and the Rapidly Exploring Random Tree (RRT) [12,13] are widely used in practice (instead of combinatorial planning approaches) to solve the motion planning problems by using collision-detection algorithms to probe and incrementally search the configuration space [14] (i.e., the space of all configurations a robot can achieve). However, they require both initial and goal configurations. Since only the goal region (i.e., the narrow gap) is known in this paper, the sampling-based approaches are not well suited. Furthermore, narrow passages in configuration space create significant difficulty [15,16] for sampling-based approaches. The performance of sampling-based algorithms often degrades significantly in such situations. Moreover, traditional sampling-based approaches may not be able to find required motions quickly enough due to the high dimensionality of the configuration space. In IMMA, a manikin model has 162 degrees of freedom (DoF) and the dimension of a configuration space is equal to the DoF.

Sampling-based approaches can be combined with local inverse kinematic methods [17], where the latter generates a robot configuration from an given end-effector goal, then the former is used to link the initial configuration to the resulting goal configuration. However, without considering to define an initial path in either $\mathbb{R}^3$ or $SE(3)$, the problem becomes more difficult than necessary to solve.

3. IMMA Manikin Modeling

In this section, we briefly describe how an IMMA manikin is modeled.

In IMMA, a manikin is represented by not only a biomechanical model, but also a collision model. The collision model uses hierarchies of rectangular swept spheres (RSS) [18] and

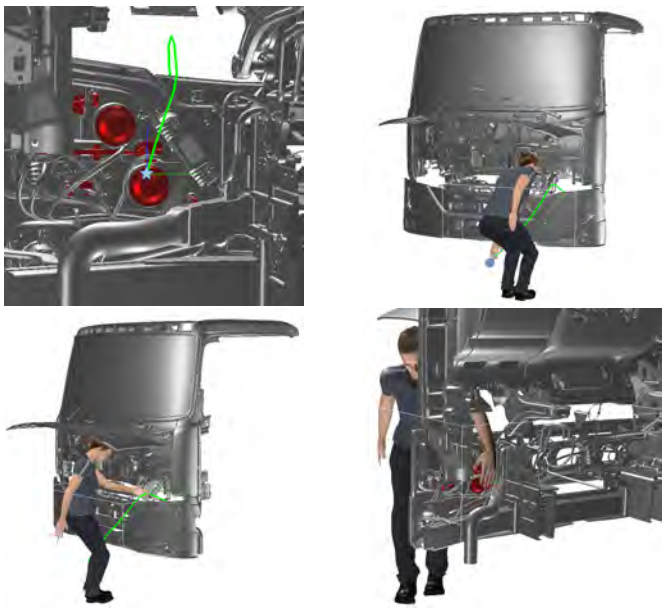

Fig. 1. UD truck headlight bulb replacement simulation. The path in green connects the initial position $\mathbf{p}_I$ (marked by the cyan star in the first subfigure) and the goal position $\mathbf{p}_G$ (marked by the cyan disc in the second subfigure). Before approaching the truck, the manikin was in a standing pose with feet together and arms by the sides. Truck CAD model courtesy of AB Volvo.

hence IMMA is able to compute signed distance between the manikin and obstacles. The IMMA biomechanical model is a hierarchy of joints and links. Each link's relative position to its parent link is determined by a rigid transformation $\mathbf{T}(\theta)$, where θ is the joint angle between the two links.

A manikin can be placed in a specific configuration (or *pose*) through forward kinematics (i.e., collect all joint angles $\boldsymbol{\theta} = [\theta_1, \theta_2, \ldots, \theta_n]$ and then calculate the corresponding transformations $\mathbf{T}_1, \mathbf{T}_2, \ldots, \mathbf{T}_n$). As previously mentioned, joint-by-joint adjustment of a manikin configuration not only is time-consuming but also produces inconsistent results. Instead, IMMA uses inverse kinematics (IK) by solving kinematic constraint equations

$$\mathbf{g}(\boldsymbol{\theta}, \mathbf{f}) = \mathbf{0}, \tag{1}$$

where $\boldsymbol{\theta}$, $\mathbf{f}$, and $\mathbf{g}$ represent joint angles, the unknown forces and moments, and a function describing the kinematic constraints, respectively. With IK, IMMA can place a finger tip at a specific position by finding a solution for Eq. 1 to obtain the joints positions that match the position of the finger tip to the target position. Consequently, a reaching movement can be achieved by simply specifying a sequence of target positions that the finger tip has to trace. In this paper, we use the tip of a hand's middle finger as the manikin's end-effector (denoted as $\mathcal{EF}$). In Fig. 1, the manikin's left hand reaches deep into the engine bay of a UD truck to replace a headlight bulb by following a computer-generated path for a sphere.

Because the number of joints exceeds the number of end-effector (i.e., a manikin's hands and feet) constraints and hence the system of equations is underdetermined, IMMA is able to take additional issues, such as ergonomics, comfort, and collision avoidance, into account when choosing a solution. To gen-

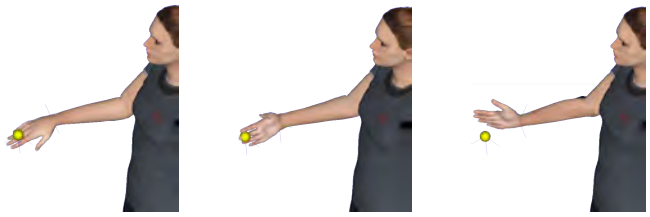

(a) −90° (b) 0° (c) 90°

Fig. 2. Pronation and supination of the right hand by rotating joint *JointRightWristRotation*.

erate human-like configurations and motions, IMMA compares many different configurations (i.e., solutions for Eq. 1) and selects the one that maximizes a scalar comfort function $h(\boldsymbol{\theta}, \mathbf{f})$. Essentially, IMMA solves the following nonlinear optimization problem

$$\begin{cases} \underset{\mathbf{x}}{\text{maximize}} & h(\mathbf{x}) \\ \text{subject to} & \mathbf{g}(\mathbf{x}) = \mathbf{0}, \end{cases} \tag{2}$$

where $\mathbf{x}^\top = [\boldsymbol{\theta}^\top, \mathbf{f}^\top]$ represent the unknowns. To prevent the manikin from coming too close to the obstacles, IMMA uses an obstacle repulsive potential field [10] and adds equations similar to the following

$$h_{ca}(\boldsymbol{\theta}) = \begin{cases} -\frac{1}{2}\eta\left(\frac{1}{d(\boldsymbol{\theta})} - \frac{1}{d^*}\right)^2 & \text{if } d(\boldsymbol{\theta}) \le d^* \\ 0 & \text{if } d(\boldsymbol{\theta}) > d^* \end{cases} \tag{3}$$

to the comfort function, where $d(\boldsymbol{\theta})$ is the signed distance between the manikin and the obstacles, d^* specifies the barrier thickness, and η is a positive scaling factor [19].

To simulate the insertion of a hand into a narrow gap, the manikin has to be able to perform two unique and important rotations of the hands: *pronation* and *supination*, in addition to its ability to move the end-effector to the target positions. The motions of pronation and supination turn the palms posteriorly (i.e., placing the palms into the prone/face-down position) and anteriorly/superiorly (i.e., placing the palms into the supine/face-up position), respectively. The IMMA manikin model introduces two joints (i.e., *JointLeftWristRotation* and *JointRightWristRotation*) to simulate pronation and supination of the hands as shown in Fig. 2. The minimum and maximum joint angles of the joints are −90° and 90°, respectively.

4. Approach

In this section, we present the problem formulation followed by a detailed description of our approach to simulate the insertion of a manikin hand into a narrow gap. Firstly, we connect a point inside the narrow gap and a point outside the narrow gap with a path in the workspace. Secondly, the manikin's end-effector (i.e., the tip of the hand's middle finger) traces the path using IK until it is close to the opening of the narrow gap. Thirdly, we perform pronation/supination and randomly shift the hand position. Fourthly, a simple but efficient test is executed to determine whether the hand is orientated and positioned correctly for the narrow gap, where the test replaces IK because it is much faster to execute. If the test passes, then the end-effector is inserted into the narrow gap using IK with the collision avoidance disabled so that it is not pushed aside by the repulsive potential field. Finally, we choose the manikin configuration (or pose) with the best clearance.

4.1. Problem formulation

Let $\mathcal{W}$ ($\mathbb{R}^3$) denote the workspace that contains a manikin and obstacles. Let C denote the configuration space (i.e., the set of all rigid-body transformations that can be applied to the manikin). Given a manikin description $\mathcal{M}$ (as a hierarchy of joints and links), a hand (left or right), an obstacle region $O \subset \mathcal{W}$, a narrow gap in the free workspace $\mathcal{W}_{free} = \mathcal{W} \setminus O$, and an initial collision-free configuration $\mathbf{q}_I$, synthesize a goal configuration $\mathbf{q}_G$ with the manikin's hand inside the narrow gap and then compute a continuous path τ: $[0, 1] \rightarrow C_{free}$ with $\tau(0) = \mathbf{q}_I$ and $\tau(1) = \mathbf{q}_G$, where the free configuration space C_{free} is defined as

$$C_{free} = \{\mathbf{q} \in C | \mathcal{M}(\mathbf{q}) \cap O = \emptyset\}. \tag{4}$$

Let $\mathbf{p} \in \mathcal{W}$ and $\phi : C \rightarrow \mathcal{W}$ denote a position in the world and the forward kinematics map, respectively. Therefore, $\mathbf{p}$ can be written as $\mathbf{p} = \phi(\mathbf{q})$, when $\mathbf{p}$ represents the position of the end-effector (i.e., the tip of the given hand's middle finger). Moreover, let $\mathbf{p}_I = \phi(\mathbf{q}_I)$ and $\mathbf{p}_G$ be a user-defined defined point inside the given narrow gap. $\mathbf{p}_I$ and $\mathbf{p}_G$ are shown in Fig. 1, although $\mathbf{p}_G$ in that figure is not inside a narrow gap. We make the simplifying assumptions that $\mathbf{p}_I$ is located in the open region just outside the narrow gap. If this assumption is not true, then the IMMA user can simply drag the target frame on the end-effector using IK until $\mathbf{p}_I$ is inside the open region.

In this paper, we assume that the hand is always flat and has the fingers together. Consequently, the displacement vectors (i.e., $\mathbf{v}_I$, $\mathbf{v}_M$, and $\mathbf{v}_R$) from the tip of the middle finger (i.e., the end-effector position) to the tips of the hand's index/middle/ring fingers are constant vectors.

4.2. Insertion of hand into narrow gap

To connect $\mathbf{p}_I$ and $\mathbf{p}_G$ with a path, we create a sphere S of diameter 10 mm [1] and define a body reference frame with its origin locating at the sphere's geometric center. After specifying a preferred clearance [21], a rigid body path planner is used to find a collision-free path for sphere S between $\mathbf{p}_I$ and $\mathbf{p}_G$ (i.e., there is no orientation constraint). The path planner will try to find a path that satisfies the given clearance, but it does not guarantee that the clearance is met. To clean up the resulting path, we perform path smoothing multiple times to obtain a continuous and smooth path τ_S. In the algorithm in Fig. 4, configuration $\mathbf{q}_I$ and path τ_S are listed as the input variables along

[1] The average width of the index finger is 16 to 20 mm for most adults [20].

with θ_{step}, n_1, and n_2, where θ_{step} is the angle step size, n_1 is the max number of valid samples of end-effector positions, and n_2 is the max number of attempts to sample end-effector positions. Next, path τ_S is discretized into N waypoints, equally spaced in terms of path length, as shown on line 1 in Fig. 4. This 3-dimensional discretized path is represented as a matrix $\mathbf{P} = [\mathbf{p}_1, \ldots, \mathbf{p}_N] \in \mathbb{R}^{3\times N}$, where $\mathbf{p}_1 = \mathbf{p}_I$ and $\mathbf{p}_N = \mathbf{p}_G$.

IK (as shown on line 6 in Fig. 5) is then applied so that the end-effector can trace the discretized path from $\mathbf{p}_1$ to $\mathbf{p}_{N-1}$ as shown on line 6 in Fig. 4. Note that IK is not required to align the end-effector's orientation to a sequence of target orientations. However, to insert the end-effector into the narrow gap, it is not sufficient to only have control over the end-effector's positions. To achieve the goal, we add a fourth DoF (i.e., pronation/supination of the arm to flip the palm either face up or face down). Unfortunately, after pronation/supination, the end-effector is no longer located at the target position as shown in Fig. 2. To move the end-effector back to the target position, IK is executed a second time (as shown on line 9 in Fig. 5). The procedure is summarized in Fig. 5. While IK ensures that the manikin's RSS models never intersect with each other to avoid self-collision, the algorithm in Fig. 5 allows the collision avoidance for obstacles to be disabled when necessary (e.g., when the hand is just outside the narrow gap and it is about to be inserted into the gap).

As the end-effector traces the discretely-sampled path (with the collision avoidance enabled), we check at each waypoint $\mathbf{p}_i$ whether $\mathbf{p}_N$ is visible from $\mathbf{p}_i$. Two waypoints $\mathbf{p}_1$ and $\mathbf{p}_2$ are considered to be visible to each other if the line segment $\overline{\mathbf{p}_1\mathbf{p}_2}$ connecting the waypoints does not collide with any obstacle (i.e., $\overline{\mathbf{p}_1\mathbf{p}_2} \cap O = \emptyset$). Let $\mathbf{p}_T$ and $\mathbf{q}_T$ denote that first waypoint on the discretized path that is visible from $\mathbf{p}_N$ (i.e., $\overline{\mathbf{p}_T\mathbf{p}_N} \cap O = \emptyset$ as shown on line 8 in Fig. 4) and the corresponding manikin configuration, respectively.

Before inserting the hand into the narrow gap, we sample two new positions (i.e., $\mathbf{p}_{TS}$ and $\mathbf{p}_{NS}$ as shown on line 20 in Fig. 4) for the end-effector in the neighborhood of $\mathbf{p}_T$ and $\mathbf{p}_N$ respectively using the algorithm in Fig. 6, where the elements (i.e., ϵ_x, ϵ_y, and ϵ_z) in the mutation vector $\boldsymbol{\epsilon}$ are normally distributed random variables with mean value 0 mm and standard deviation 10 mm. Given the end-effector positions $\mathbf{p}_{TS}$ and $\mathbf{p}_{NS}$ plus the displacement vectors (i.e., $\mathbf{v}_I$, $\mathbf{v}_M$, and $\mathbf{v}_R$), we can easily obtain the corresponding positions of the tips of the index/middle/ring fingers and the line segments between them. Next, we perform a quick test to verify whether the hand after the random shifting is positioned and oriented correctly for the narrow gap by mapping line segment $\overline{\mathbf{p}_T\mathbf{p}_N}$ to these newly created line segments as shown in Fig. 3 and looking for collisions with the obstacles during the mapping process (as shown on line 15 in Fig. 6). If collision occurs, then the combination of the pronation/supination and the random shifting is considered to be bad and discarded.

If the hand after the random shifting is positioned and oriented correctly for the narrow gap, we divide the line segment $\overline{\mathbf{p}_{TS}\mathbf{p}_{NS}}$ into a series of waypoints connected by line segments and then let the end-effector trace the waypoints using IK, but with collision avoidance disabled this time. If the collision avoidance remains enabled, the end-effector will likely be unable to enter the narrow gap due to the obstacle repulsive potential field. At each waypoint, we compute the signed distance between the manikin and the obstacles. We synthesize

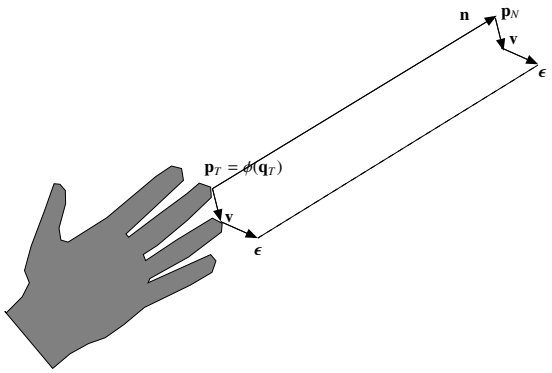

Fig. 3. Shift the end-effector position randomly.

also the manikin motions between two adjacent waypoints by linearly interpolating between the manikin states at these two waypoints and compute the corresponding signed distance as shown on line 28 in Fig. 4. If the distance is less than zero, the manikin collision model and the obstacles penetrate each other. The algorithm in Fig. 4 returns the manikin configuration sequence with the least penetration. The manikin configurations at the end of the sequence are not guaranteed to be collision-free because the end-effector is located inside the narrow gap then and the collision avoidance has been disabled. To obtain a collision-free sequence of manikin configurations, we simply remove all configurations between the first one in collision and the last one in the sequence.

Since collision avoidance is turned off when the end-effector is moved along the line segment $\overline{\mathbf{p}_{TS}\mathbf{p}_{NS}}$, the last configuration in the sequence can be improved by enabling the collision avoidance again and then dragging the end-effector forward towards $\mathbf{p}_N$ with the aim of (1) maximize the clearance; (2) move the end-effector as deep as possible into the narrow gap. We are able to turn on the collision avoidance again, because the end-effector is most likely already inside the narrow gap and hence it won't be rejected by the obstacle repulsive potential field.

5. Experiments

In this section, we evaluate the algorithm with two experiments, where the manikin has to insert a hand into two narrow gaps from two different car models. In each experiment, the manikin is placed manually by the IMMA user in the neighborhood of the narrow gap such that the gap is reachable by the right hand. Once the manikin is in place, the right foot of the manikin is locked by the IMMA user to its current position, although it is still allowed to rotate around the axis vertical to the ground surface. The following values were used in all experiments: $n_1 = 10$, $n_2 = 100$, and $\theta_{step} = 5°$. We ran the simulations on a Windows 10 PC with 16 GB RAM and a Intel Core i7-4770 CPU with four cores and a clock speed of 3.40 GHz, although we did not parallelize the algorithm presented in this paper and hence it was not executed concurrently.

In the first experiment, the manikin has to insert its right hand into a narrow gap between two gray-colored pipes next to the radiator/condenser combo (Fig. 7). The shortest distance between the two pipes is about 32 mm, whereas the shortest distance between the silver-colored ring around the lower pipe and the cyan-colored fastener around the pipe above is about

Input:
θ_{step}: angle step size
n_1: max number of valid samples of end-effector positions
n_2: max number of attempts to sample end-effector positions
Configuration $\mathbf{q}_I$: manikin's initial configuration
Path τ_S: a collision-free path between $\mathbf{p}_I$ and $\mathbf{p}_G$ for sphere S
Output:
$\mathbf{Q}$: a sequence of manikin configurations that takes $\mathcal{EF}$ from $\mathbf{p}_I$ to region around $\mathbf{p}_G$

$(\mathbf{p}_1, \ldots, \mathbf{p}_N) \leftarrow$ discretize path τ_S
for $\theta = -90°$ to $90°$ stepsize θ_{step} **do**
  $visible \leftarrow false$
  $\mathbf{q}_T \leftarrow \mathbf{q}_I$
  for each $\mathbf{p} \in (\mathbf{p}_1, \ldots, \mathbf{p}_{N-1})$ **do**
    $\mathbf{q}_T \leftarrow$ PredictManikinConfig($\mathbf{q}_T$, $\mathbf{p}$, θ, $true$)
    $\mathbf{p}_T \leftarrow \phi(\mathbf{q}_T)$
    if $\overline{\mathbf{p}_T\mathbf{p}_N} \cap \mathcal{O} = \emptyset$ **then**
      $visible \leftarrow true$
      break
    end if
  end for
  if $visible = false$ **then**
    continue
  end if
  for $i = 1$ to n_1 **do**
    $j \leftarrow 0$
    $(\mathbf{p}_{TS}, \mathbf{p}_{NS}) \leftarrow (\mathbf{0}, \mathbf{0})$
    do
      $(\mathbf{p}_{TS}, \mathbf{p}_{NS}) \leftarrow$ SampleEndEffectorPositions($\mathbf{p}_T$, $\mathbf{p}_N$)
      $j \leftarrow j + 1$
    while $j < n_2 \wedge (\mathbf{p}_{TS}, \mathbf{p}_{NS}) \neq (\mathbf{0}, \mathbf{0})$
    if $(\mathbf{p}_{TS}, \mathbf{p}_{NS}) \neq (\mathbf{0}, \mathbf{0})$ **then**
      $negDistSum \leftarrow 0.0$
      for $t \in (0.0, \ldots, 1.0)$ **do**
        $\mathbf{p} \leftarrow \mathbf{p}_{TS} + t * (\mathbf{p}_{NS} - \mathbf{p}_{TS})$
        $\mathbf{q}_T \leftarrow$ PredictManikinConfig($\mathbf{q}_T$, $\mathbf{p}$, θ, $false$)
        $minDist \leftarrow$ compute signed distance to obstacles at $\mathbf{q}_T$
        if $minDist < 0.0$ **then**
          $negDistSum = negDistSum + minDist$
        end if
      end for
    end if
  end for
end for
$\mathbf{Q} \leftarrow$ configuration sequence with the maximum $negDistSum$
return $\mathbf{Q}$

Fig. 4. Synthesize the goal configuration inside the narrow gap and the collision-free path between the initial and goal configurations

Input:
Configuration $\mathbf{q}_{IN}$: manikin's current configuration
Position $\mathbf{p}_{TARGET}$: target position for $\mathcal{EF}$
Angle θ: rotation angle for Joint(Left|Right)WristRotation $\mathcal{J}$
Boolean $colliAvoid$: enable collision avoidance for the obstacles
Output:
Configuration $\mathbf{q}_{OUT}$: the resulting manikin configuration

procedure PredictManikinConfig($\mathbf{q}_{IN}$, $\mathbf{p}_{TARGET}$, θ, $colliAvoid$)
  if $colliAvoid = false$ **then**
    Exclude obstacles from collision avoidance when solving Eq. 2
  end if
  Set manikin configuration to $\mathbf{q}_{IN}$
  Move $\mathcal{EF}$ to $\mathbf{p}_{TARGET}$ and $\mathbf{I}_3$ by solving Eq. 2
  Rotate $\mathcal{J}$ by θ
  $\mathbf{R}_{EF} \leftarrow$ orientation of $\mathcal{EF}$
  $\mathbf{q}_{OUT} \leftarrow$ Move $\mathcal{EF}$ to $\mathbf{p}_{TARGET}$ and $\mathbf{R}_{EF}$ by solving Eq. 2
  return $\mathbf{q}_{OUT}$
end procedure

Fig. 5. Predict manikin configuration

Input:
Positions $\mathbf{p}_T$ and $\mathbf{p}_N$ ▷ See Fig. 4
Output:
Positions $(\mathbf{p}_{TS}, \mathbf{p}_{NS})$: newly sampled end-effector positions

procedure SampleEndEffectorPositions($\mathbf{p}_T$, $\mathbf{p}_N$)
  $\mathbf{n} \leftarrow \mathbf{p}_N - \mathbf{p}_T$
  $\boldsymbol{\epsilon} \leftarrow [\epsilon_x \quad \epsilon_y \quad \epsilon_z]^\intercal$
  for each $\mathbf{v} \in (\mathbf{v}_I, \mathbf{v}_M, \mathbf{v}_R)$ **do**
    $\Pi_1 \leftarrow$ plane with normal $\mathbf{n}$ through point $\mathbf{p}_T + \mathbf{v}$
    $\Pi_2 \leftarrow$ plane with normal $\mathbf{n}$ through point $\mathbf{p}_N + \mathbf{v}$
    $\mathbf{p}_{\Pi_1} \leftarrow$ project point $\mathbf{p}_T + \mathbf{v} + \boldsymbol{\epsilon}$ onto Π_1
    $\mathbf{p}_{\Pi_2} \leftarrow$ project point $\mathbf{p}_N + \mathbf{v} + \boldsymbol{\epsilon}$ onto Π_2
    if $\mathbf{v} = \mathbf{v}_M$ **then**
      $(\mathbf{p}_{TS}, \mathbf{p}_{NS}) \leftarrow (\mathbf{p}_{\Pi_1}, \mathbf{p}_{\Pi_2})$
    end if
    for $t \in (0.0, \ldots, 1.0)$ **do**
      $\mathbf{p}_1 \leftarrow \mathbf{p}_T + t * (\mathbf{p}_{\Pi_1} - \mathbf{p}_T)$
      $\mathbf{p}_2 \leftarrow \mathbf{p}_N + t * (\mathbf{p}_{\Pi_2} - \mathbf{p}_N)$
      if $\overline{\mathbf{p}_1\mathbf{p}_2} \cap \mathcal{O} \neq \emptyset$ **then**
        return $(\mathbf{0}, \mathbf{0})$ ▷ Failed to sample new positions
      end if
    end for
  end for
  return $(\mathbf{p}_{TS}, \mathbf{p}_{NS})$
end procedure

Fig. 6. Sample end-effector positions

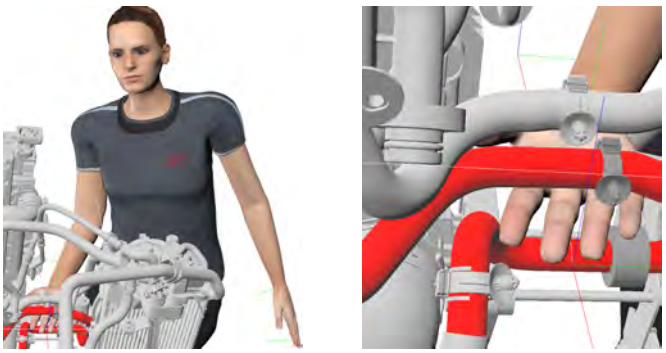

Fig. 7. Insertion of right hand (with the palm facing up) into a narrow gap between two pipes in Volvo XC90 engine bay. Car CAD model courtesy of Volvo Cars.

Table 1. Results obtained from planning the insertion of the manikin hand into two narrow gaps.

Scenario	EXP 1 (XC90)	EXP 2
Number of successful plans	5/5	5/5
Avg. planning time (sec)	302.2 ± 8.6	280.6 ± 5.2

18 mm. To orientate the hand for the narrow gap, the algorithm in Fig. 4 performs pronation and supination to place the palm into the face-down and face-up positions, respectively. The best solution found by the algorithm places the palm into the face-up position as shown in Fig. 7.

In the second experiment, the manikin has to insert its right hand into a narrow gap between a compression fitting connecting two vertical pipes and a vertical flat surface, where the top of the narrow gap is blocked by a bracket, but the bottom of the narrow gap is open. The width of the narrow opening formed by the compression fitting, the flat surface, and the bracket is about 19 mm.

Table 1 shows the results obtained from these experiments. When collecting the data, all solutions were found by searching between $-90°$ and $90°$. Success of an experiment run implies that (1) the generation of a collision-free goal configuration with the hand inside the narrow gap; (2) the generation of a collision-free path from the initial configuration to the goal configuration. At the end of each experiment run, we verify manually whether the hand is inside the narrow gap or not.

6. Discussion

As a first step, when we ran the experiments, we had to manually select one hand that we wanted to insert into the narrow gap after setting the manikin's initial configuration. A possibility for the future work is to automatically choose one hand for the task based on the reachabilities of both arms [22].

Secondly, instead of searching between $-90°$ and $90°$, a narrower range of angles can be specified instead to (1) obtain the desired hand pose; (2) speed up the search. For example, the palm is facing up in Fig. 7 because we searched between $-90°$ and $90°$. If the face-down position (Fig. 8) is preferred for the palm, we can set the maximum joint angle to for example $-70°$ instead of $90°$. When the palm is facing down, the thumb is blocked by the silver-colored ring around the lower pipe as

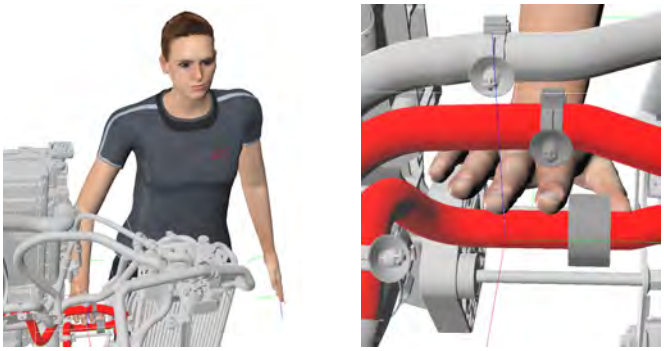

Fig. 8. Insertion of right hand (with the palm facing down) into a narrow gap between two pipes in Volvo XC90 engine bay. Car CAD model courtesy of Volvo Cars.

shown in Fig. 8 and hence the hand is not inserted into the gap as far as when the palm is facing up. Similarly, if the narrow gap has a vertical opening, we can speed up the computation by searching for example between $-30°$ and $30°$ instead of between $-90°$ and $90°$.

Thirdly, as mentioned in Section 4, the end-effector traces a discretely-sampled path. When the end-effector is close to the narrow gap, the collision avoidance is disabled so that the end-effector won't be pushed aside by the repulsive potential field. Instead, we compute the signed distance between the manikin and the obstacles to check whether they are in collision or not at each waypoint and between two consecutive waypoints by linearly interpolating between them to calculate a continuous-time path. However, the manikin might still collide with thin obstacles when tracing the resulting path. To enforce the continuous-time safety of the path, we can calculate the signed distance between the swept-out volume of the manikin RSS and the obstacles instead [23].

Fourthly, we could set n_1 to for example 5 instead of 10 to speed up the search. Once the angle with the best goal configuration is identified, we can sample additional valid end-effector positions at that angle and then try to find better goal configurations.

Fifthly, a single goal configuration is synthesized in Section 4. We could present the top n goal configurations to the IMMA user instead and let him/her choose one configuration for the next task he/she wants to simulate. For example, the IMMA user can drag the hand even deeper into the narrow gap and then close the hand to perform a grasp.

Finally, we would like to speedup the algorithm presented in this paper by searching in parallel for appropriate angle values.

7. Conclusions

We have presented an algorithm that explores the 4D space (position of a fingertip plus pronation/supination of the arm) to simulate an assembly with narrow insertion clearances. The planner takes a user-specified goal position inside a narrow gap as its input and then synthesizes not only a goal configuration with the hand inside the narrow gap, but also a path from the manikin's initial configuration to the resulting goal configuration. We have evaluated the algorithm with two simulation examples from the vehicle industry. In the future, we would like to extend the approach to the case where a worker's hand holds a tool.

References

[1] A.-C. Falck, R. Örtengren, D. Högberg, The impact of poor assembly ergonomics on product quality: A costbenefit analysis in car manufacturing, Human Factors and Ergonomics in Manufacturing and Service Industries 20 (1).

[2] D. Högberg, L. Hanson, B. R., J. S. Carlson, Creating and shaping the dhm tool imma for ergonomic product and production design, International Journal of the Digital Human 1 (2).

[3] H. Choset, K. M. Lynch, S. Hutchinson, et al., Principles of Robot Motion: Theory, Algorithms, and Implementations, The MIT Press, 2005.

[4] U. Gaur, A. Jain, S. Goel, Towards Real-Time Monocular Video-Based Avatar Animation, Springer, Berlin, Heidelberg, 2008.

[5] D. B. Chaffin, Improving digital human modelling for proactive ergonomics in design, Ergonomics 48 (5).

[6] A. Keyvani, Structuring and use of motion data for computer manikin work task simulations, Ph.D. thesis, Department of Product and Production Development, Chalmers University of Technology (2014).

[7] A. Sudsang, J. Ponce, N. Srinivasa, Grasping and in-hand manipulation: Geometry and algorithms, Algorithmica 26 (3) (2000) 466–493.

[8] Y. Li, J. P. Saut, J. Pettré, A. Sahbani, F. Multon, Fast grasp planning using cord geometry, IEEE Transactions on Robotics 31 (6).

[9] Y. Park, J. Lee, J. Bae, Development of a wearable sensing glove for measuring the motion of fingers using linear potentiometers and flexible wires, IEEE Transactions on Industrial Informatics 11 (1).

[10] O. Khatib, Real-time obstacle avoidance for manipulators and mobile robots, The International Journal of Robotics Research 5 (1).

[11] L. E. Kavraki, P. Svestka, J. C. Latombe, M. H. Overmars, Probabilistic roadmaps for path planning in high-dimensional configuration spaces, IEEE Transactions on Robotics and Automation 12 (4).

[12] J. J. Kuffner, S. M. LaValle, RRT-connect: An efficient approach to single-query path planning, in: Proceedings of the 2000 IEEE International Conference on Robotics and Automation (ICRA), 2000.

[13] S. M. LaValle, J. James J. Kuffner, Randomized kinodynamic planning, The International Journal of Robotics Research 20 (5).

[14] T. Lozano-Perez, Spatial planning: A configuration space approach, IEEE Transactions on Computers C-32 (2).

[15] D. Hsu, T. Jiang, J. Reif, Z. Sun, The bridge test for sampling narrow passages with probabilistic roadmap planners, in: Proceedings of the 2003 IEEE International Conference on Robotics and Automation (ICRA), Vol. 3, 2003.

[16] J. Lee, O. Kwon, L. Zhang, S. E. Yoon, A selective retraction-based RRT planner for various environments, IEEE Transactions on Robotics 30 (4).

[17] K. Shankar, J. W. Burdick, N. H. Hudson, A quadratic programming approach to quasi-static whole-body manipulation, in: Algorithmic Foundations of Robotics XI. Springer Tracts in Advanced Robotics, no. 107, Springer, 2015.

[18] E. Larsen, S. Gottschalk, M. C. Lin, D. Manocha, Fast distance queries with rectangular swept sphere volumes, in: Proceedings of the 2000 IEEE International Conference on Robotics and Automation (ICRA), Vol. 4, 2000.

[19] R. Bohlin, N. Delfs, L. Hanson, D. Högberg, J. S. Carlson, Automatic creation of virtual manikin motions maximizing comfort in manual assembly processes, in: Proceedings of the 4th CIRP Conference on Assembly Technology and Systems (CATS), Ann Arbor, USA, 2012.

[20] K. Dandekar, B. I. Raju, M. A. Srinivasan, 3-D finite-element models of human and monkey fingertips to investigate the mechanics of tactile sense, Journal of Biomechanical Engineering 125 (5).

[21] R. Geraerts, M. H. Overmars, On improving the clearance for robots in high-dimensional configuration spaces, in: Proceedings of the 2005 IEEE/RSJ International Conference on Intelligent Robots and Systems, 2005.

[22] N. Vahrenkamp, T. Asfour, R. Dillmann, Robot placement based on reachability inversion, in: Proceedings of the 2013 IEEE International Conference on Robotics and Automation (ICRA), 2013.

[23] Y. Duan, S. Patil, J. Schulman, K. Goldberg, P. Abbeel, Planning locally optimal, curvature-constrained trajectories in 3d using sequential convex optimization, in: Proceedings of the 2014 IEEE International Conference on Robotics and Automation (ICRA), 2014.